*Journal of Applied Mechanics and Technical Physics, Vol. 47, No. 2, pp. 298–305, 2006*

# TYPES OF LOCALIZATION OF PLASTIC DEFORMATION AND STAGES OF LOADING DIAGRAMS OF METALLIC MATERIALS WITH DIFFERENT CRYSTALLINE STRUCTURES

**V. I. Danilov, L. B. Zuev, E. V. Letakhova, D. V. Orlova, and I. A. Okhrimenko**

UDC 669.017:539.213

*Macrolocalization, which accompanies the process of plastic deformation beginning from the yield point and ending by fracture, is determined by the staged character of material-loading diagrams. The evolution of localization patterns in a plastic flow of body-centered cubic vanadium alloy, hexagonal close-packed magnesium alloy, tetragonal tin, and face-centered cubic submicrocrystalline aluminum is analyzed within this concept.*

**Key words:** *plastic deformation, fracture, macrolocalization, autowaves, stages of loading diagrams.*

**Introduction.** It was found [1–3] that macrolocalization accompanies the process of shape variation of all materials, independent of their chemical nature, crystallographic state, and real structure, over the entire process from the yield point to fracture. The types of deformation localization have a uniform dependence on the law of strain hardening of the material (loading diagram) and uniformly change from one stage to another. The number of such types is limited. Four types are known at the moment [3]:

1) single moving deformation fronts (autowaves of excitation or switching);
2) equidistant moving zones of deformation localization (phase autowave);
3) spatially periodic steady distributions of deformation-localization sites (stable dissipative structures);
4) high-amplitude motionless deformation sites.

The first type is typical of stages of easy slip of single crystals and yield areas of polycrystalline materials. The stages of linear hardening correspond to the second type of localization in the form of phase autowaves. The third type of localization arises at stages of parabolic hardening. High-amplitude steady zones of deformation localization in regions of future viscous fracture were observed when the strain before the beginning of neck formation was several percent of the total strain.

The evolution of localization patterns rigorously follows the stages of the strain curves. If some stage is absent, the corresponding type of localization is absent as well. Therefore, it was only the third type of macrolocalization that was observed in all experiments without any exceptions, which were performed with single and polycrystals, pure metals and high alloys, ordered structures, materials with dislocation and twinning mechanisms of deformation, alloys with phase-change plasticity, and substances with viscous and quasi-brittle fracture [3]. The phenomenology of transformation of the first to the second type of localization [4] and from the second to the third type of localization [5] has been described. It remains unclear, however, how a steady dissipative structure (third type) is transformed to a distribution with one high-amplitude maximum.

Institute of Strength Physics and Material Science, Siberian Division, Russian Academy of Sciences, Tomsk 634021; dvi@ispms.tsc.ru. Translated from Prikladnaya Mekhanika i Tekhnicheskaya Fizika, Vol. 47, No. 2, pp. 176–184, March–April, 2006. Original article submitted May 5, 2005.

 

TABLE 1

| Material | Structure | Grain size, $\mu$m | Chemical composition, % | | | | | | | | | | |
|---|---|---|---|---|---|---|---|---|---|---|---|---|---|
| | | | V | Mg | Sn | Al | Zr | Si | Mn | C | Ce | Zn | Other elements |
| 1. V–Zr–C alloy | b.c.c. | 5 | >97.0 | — | — | — | 2.3 | — | — | 0.4 | — | — | <0.3 |
| 2. Mg–Mn–Ce alloy | h.c.p. | 12.5 | — | >97.0 | — | 0.1 | 0.1 | 0.1 | 1.3 to 2.2 | — | 0.15 to 0.35 | 0.3 | <0.3 |
| 3. Tin $\beta$-Sn | b.c.t. | $1.2 \cdot 10^3$ | — | — | 99.999 | $<3 \cdot 10^{-4}$ | — | — | — | — | — | $3 \cdot 10^{-5}$ | $<7 \cdot 10^{-4}$ |
| 4. Submicrocrystalline aluminum | f.c.c. | 0.03 to 0.1 | 0.005 | 0.002 | — | 99.83 | — | 0.15 | 0.003 | — | — | 0.008 | $<2 \cdot 10^{-3}$ |

Wave processes at stages of linear hardening and the phenomenon of association of deformation-localization sites at the place of future fracture observed on the portions of the strain curves with hardening exponents $n > 1/2$ are analyzed in the present paper.

**Materials and Experimental Procedures.** The basic criterion of choosing the materials for the present study was the type of the strain curve, which should contain all hardening stages if possible. Another important factor was the fact that most material examined previously had an face-centered cubic (f.c.c.) structure. It should be noted that the basic concepts of the stages of the strain curves of polycrystalline materials have been already formed by the end of the 1970s [6–9]. In the general case, the loading diagrams of polycrystals consist of the initial transitional stage I, linear stage II, and parabolic stage III, where $\sigma \sim \varepsilon^n$. Taylor [10] thought that $n = 1/2$ at this stage. In soft types of deformation (compression or rolling), a specific stage (IV) is sometimes observed as well [9]. The transitional stage can have either an increasing or a decreasing hardening rate and normally is not very long. The duration of the linear stage depends on numerous structural factors (type of the crystalline lattice, orderliness of solid solutions, grain size, etc.). It was shown [11] that the duration of the transitional stage increases and the duration of the linear stage decreases with increasing grain size in polycrystalline aluminum. At a certain size of structural elements, the linear stage disappears altogether. In body-centered cubic (b.c.c.) and hexagonal close-packed (h.c.p.) materials, stage III has a complicated structure. It is divided into several substages with hardening exponents $n < 1/2$ [12, 13], which actually reflects the delayed transition from the visible uniform deformation to the formation of a fracture neck.

Based on the considerations described above, we examined materials whose chemical composition and structural state are listed in Table 1.

Flat samples of the "double blade" type with the working section size of $40 \times 6 \times 1$ mm were used in all cases. The samples were stamped from cold-rolled plates so that the longitudinal axis coincided with the rolling direction. The samples of chemically pure tin were not thermally treated after their manufacturing, whereas the samples of the MA8 commercial magnesium alloy and the experimental vanadium alloy were subjected to recrystallization annealing. The submicrocrystalline structure of aluminum was formed by the method of equal-channel angular pressing of $50 \times 15 \times 15$ mm billets of A85 commercial pure aluminum. After pressing, the billets with the submicrocrystalline structure were rolled at room temperature into sheets 1 mm thick, which were then used to stamp the samples. The test scheme for all materials implied active extension with a constant velocity of $8.33 \cdot 10^{-5}$ sec$^{-1}$ at room temperature.

The strain curves for the materials considered are plotted in Fig. 1. The diagrams for the b.c.c. vanadium alloy (curve 1) and body-centered tetragonal (b.c.t.) tin (curve 3) refer to the most widespread type, where the transitional stage is rather short and has an increasing hardening rate. For the h.c.p. MA8 alloy (curve 2), vice

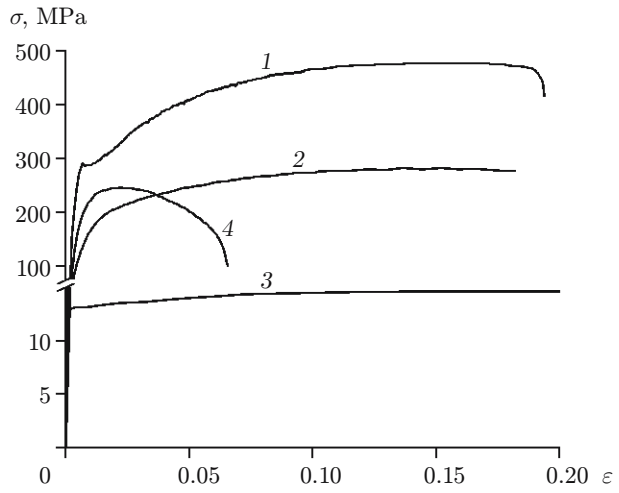


Fig. 1. Strain curves for V–Zr–C (1), Mg–Mn–Ce (2), Sn (3), and Al (4).

versa, the transitional stage is rather long, and the entire strain curve resembles a parabola. Finally, the diagram of deformation of submicrocrystalline aluminum at the ascending segment (up to a conventional ultimate strength $\sigma_{\rm B}$) is the same as that for MA8, but then the material is deformed in the neck for a long time with decreasing conventional stress. Accumulation of the total strain $\varepsilon_{\rm tot}$ on the ascending branch here is half that on the descending branch (curve 4).

The stages of the strain curves were analyzed in the coordinates $s \sim e$, where $s = \sigma(1+\varepsilon)$ is the true stress and $e = \ln(1+\varepsilon)$ is the true strain. For the V–Zr–C alloy and $\beta$-Sn, the strain curves were reconstructed to the coordinates $s \sim e^{1/2}$ under the assumption of Taylor's law of hardening. In this representation, the stage of linear hardening has the form of a quadratic parabola and is clearly identified on the background of other (close to linear) segments of the diagram. Application of this procedure allowed us to state that the linear stage II in the vanadium alloy is within $0.0095 \leqslant \varepsilon \leqslant 0.039$. This stage is characterized by the hardening rate $\theta = \partial\sigma/\partial\varepsilon = 1640$ MPa. The remaining part of the diagram consists of several straight-line segments. It is impossible to exactly identify them, and one should perform a logarithmic linearization, using Honeycomb's representation [10] according to which the strain curve of a polycrystal can be described as

$$s = s_0 + Ke^n,$$

where $s_0$ is the critical shear stress for the polycrystal and $n \leqslant 1$. The hardening exponents $n$ are different at different stages of the diagram; stage III is divided into several substages, which are clearly identified by means of linearization in the logarithmic coordinates $\ln(s - s_0) \sim \ln(e)$. Thus, it was found that the parabolic stage in the vanadium alloy consists of two substages with $n_1 = 0.48$ and $n_2 = 0.38$. The durations of the first and second substages are $0.041 \leqslant \varepsilon \leqslant 0.074$ and $0.077 \leqslant \varepsilon \leqslant 0.098$, respectively. A similar treatment of the strain curve for tin made it possible to identify the linear stage in the interval $0.01 \leqslant \varepsilon \leqslant 0.072$. The hardening rate at this stage is very small and reaches only $\theta = 33$ MPa. The remaining part of this diagram is adequately interpolated by a parabola with $n \approx 1/2$, at least up to $\varepsilon = 0.3$.

The magnesium alloy has no yield area; hence, we can assume that $s_0 = \sigma_{0.2}$ and perform linearization with logarithmic coordinates for the entire loading diagram at once. Then, the diagram is divided into three straight-line segments. The hardening exponents in these segments are $n_L = 0.98$ in the interval $0.011 \leqslant \varepsilon \leqslant 0.024$, $n_1 = 0.57$ in the interval $0.024 \leqslant \varepsilon \leqslant 0.054$, and $n_2 = 0.43$ in the interval $0.058 \leqslant \varepsilon \leqslant 0.12$. Thus, the first segment is the linear stage with the hardening exponent close to unity, and two other segments are two parabolic substages. The slope of the first segment allowed determining the hardening rate at the linear stage: $\theta = \partial\sigma/\partial\varepsilon = 850$ MPa.

For aluminum, the reconstruction to true stresses and true strains is possible on the ascending branch only. The analysis of the stages was performed by the same method as that used for the magnesium alloy. It turned out that the entire ascending branch is adequately interpolated by a parabola with an exponent $n \approx 1/2$. The descending branch describes the geometric softening, and one should formally assume that $n < 0$.

Registration and analysis of localization patterns were performed by recording the fields of displacements of the points of the deformed sample by the method of double-exposure speckle interferometry, which was described in detail, e.g., in [1], with a step of 0.2% of the total conventional strain $\varepsilon_{\text{tot}}$. Numerical differentiation of the displacement fields over the coordinates allows us to determine all components of the distortion tensor for the two-dimensional case at an arbitrary point of the extended sample: local elongation $\varepsilon_{xx}$, local restriction $\varepsilon_{yy}$, local shear $\varepsilon_{xy}$, and local rotation $\omega_z$. Thus, the zones of macrolocalization are most clearly identified in considering local elongations as high and sharp peaks of $\varepsilon_{xx}$ (Fig. 2). To study the kinetics of the evolution of macrolocalization patterns, we used the representation of $X$ local sites in the sample as a function of strain or time (under active extension, $\varepsilon \sim t$). It was shown [14] that such a procedure applied to distributions with spatial–temporal periodicity (wave distributions) makes it possible to determine the spatial $\lambda$ and temporal $T$ periods of the process and also the velocity of deformation sites $V = dX/dt$.

**Basic Results.** Figure 3a shows the dependences $X(t)$ for the process of deformation of the vanadium alloy in the interval of the total conventional strain $0.01 \leqslant \varepsilon \leqslant 0.1$, which corresponds to the deformation time period of 125 to 1250 sec. (Hereinafter, we used the linear interpolation by the least squares technique.) We can clearly identify three time intervals where the types of localization patterns are drastically different. In the interval of 150 to 475 sec, four equidistant deformation sites move with almost constant velocities, i.e., the wave process with $\lambda_{\text{II}} = 4.5 \pm 0.5$ mm, $T_{\text{II}} = 67$ sec, and $V_{\text{II}} = 6.7 \cdot 10^{-5}$ m/sec occurs ($\lambda_{\text{II}}$, $T_{\text{II}}$, and $V_{\text{II}}$ are the mean values of the length, period, and velocity of the phase autowave, respectively). Then, there follows a spatially periodic steady process with almost the same characteristic size $\lambda_{\text{III}} = 5 \pm 0.5$ mm in the interval from 540 to 800 sec. Finally, in the interval from 820 to 980 sec, only one localization zone with the coordinate $X_{\text{f}} = 15$ mm remains motionless, and all the other sites move to approach this zone.

In the case of deformation of the magnesium alloy (Fig. 3b), we analyzed the evolution of localization patterns in the same interval of the total conventional strain $0.01 \leqslant \varepsilon \leqslant 0.1$. In the time interval from 130 to 300 sec, an autowave wave process with $\lambda_{\text{II}} = 6.5 \pm 0.5$ mm, $T_{\text{II}} = 135$ sec, and $V_{\text{II}} = 4.8 \cdot 10^{-5}$ m/sec is observed. The segment of the transition to a spatially periodic steady pattern is shorter. This type of localization with $\lambda_{\text{III}} = 7 \pm 0.5$ mm arises already by the time $t = 330$ sec from the beginning of loading and is retained up to $t = 650$ sec. Then, the localization zone with the coordinate $X_{\text{f}} \approx 37$ mm becomes prevailing and almost steady. The remaining localization sites move so that they reach the steady zone by the time $t_{\text{f}}* \approx 1270$ sec from the beginning of loading. It should be noted that sample fracture occurred at $t_{\text{f}} = 1302$ sec after the beginning of deformation, and this happened in the cross section with the coordinate $X_{\text{f}} = 37$ mm.

The evolution of the distribution of localization sites in submicrocrystalline aluminum is shown in Fig. 3c. From $t = 50$ sec to $t = 185$ sec from the beginning of loading, three steady deformation sites are observed. Two of them become moving by the time $t = 260$ sec from the beginning of deformation. As in the V–Zr–C and MA8 alloys, they move toward the remaining steady maximum $\varepsilon_{xx}$ whose coordinate is $X_{\text{f}} = 34$ mm. The amplitude of the lower site rapidly decreases, and it ceases to exist by the time $t = 325$ sec. Yet, both this site and the next one, if they moved with constant velocities, would reach the steady zone at the time $t = 740$ sec from the beginning of deformation. The fracture occurred at the time $t = 732$ sec in the cross section with the coordinate $X_{\text{f}}* = 33.5$ mm.

The study of the positions of localization zones during tin deformation showed that the wave process with the parameters $\lambda_{\text{II}} = 4 \pm 0.5$ mm, $T_{\text{II}} = 55$ sec, and $V_{\text{II}} = 7.3 \cdot 10^{-5}$ m/sec also occurs in the time interval from 125 to 875 sec. Then, a steady system of equidistant deformation sites with a spatial period $\lambda_{\text{III}} \approx 4.5$ mm is formed. Further deformation in the examined interval of the total strain $\varepsilon$ does not alter the localization type. A possible reason is that the parabolic stages with hardening exponents other than 1/2 were left outside the scope of the present study. As was noted above, deformation localization in Sn was considered in the interval $0 < \varepsilon < 0.3$, and the total elongation at the fracture moment could exceed 10%.

**Analysis of Results.** As was noted above, waves of localization of macrodeformation were observed previously at the stages of linear hardening for most f.c.c. pure metals and high alloys. They were interpreted as the result of self-organization in open systems consisting of the sample and the loading device, i.e., as autowaves. In the present work, the autowave character of localization was also observed in all cases with the stage of linear hardening: in Mg–Mn–Ce and V–Zr–C alloys and in pure Sn, though their crystallographic structure is absolutely different. According to [14], f.c.c. materials have an inversely proportional dependence of localization autowave velocity $V_{\text{II}}$ on the hardening rates $\theta$ at the linear stage II normalized to shear moduli. The form of the dependence

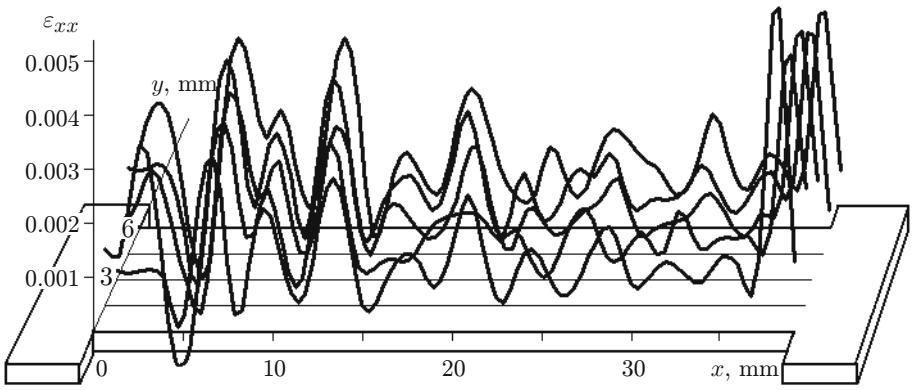


Fig. 2. Distribution of local elongations over the sample of the magnesium alloy ($\varepsilon = 0.016$).

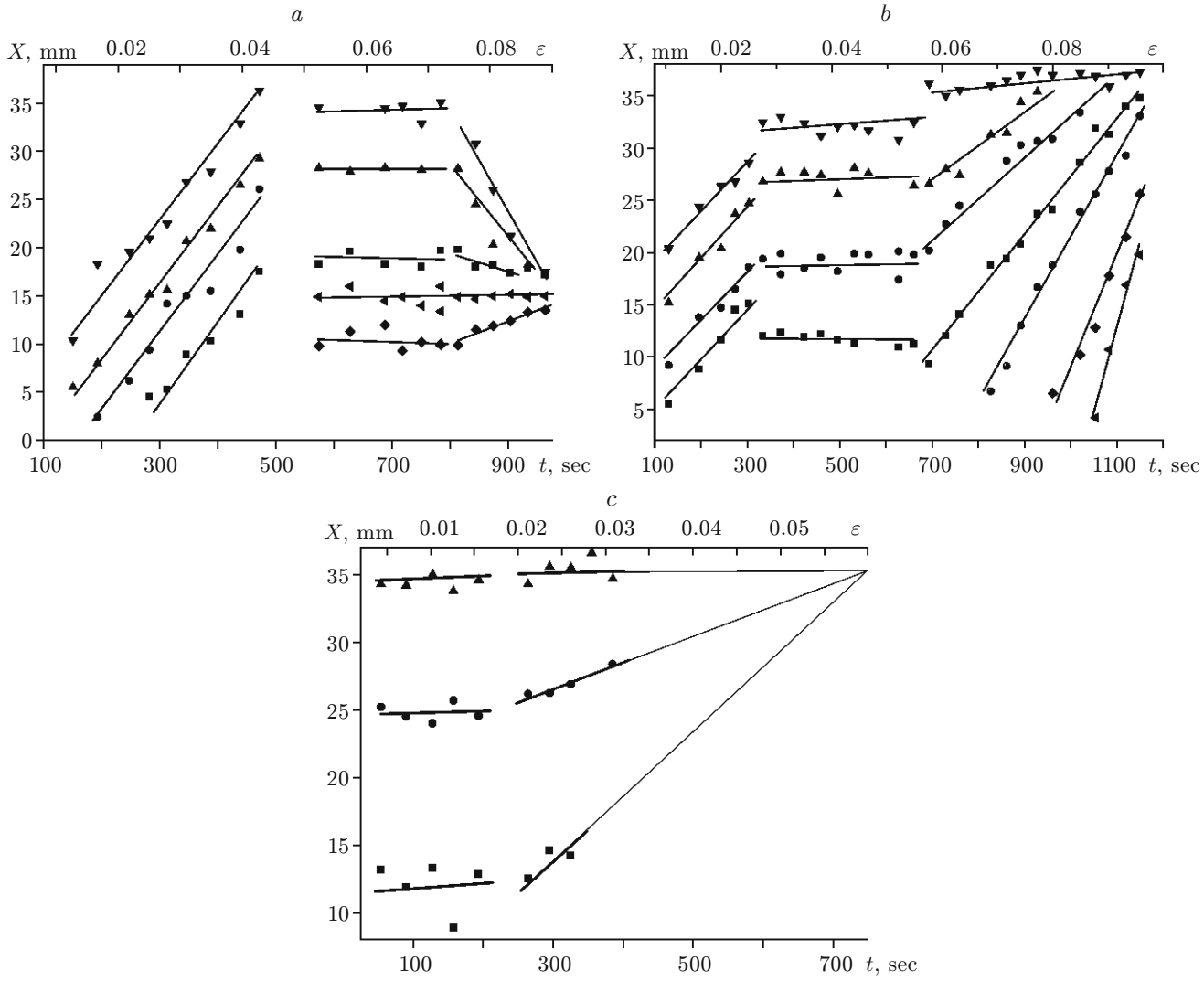


Fig. 3. Kinetics of the localization process during deformation of the V–Zr–C alloy (a), Mg–Mn–Ce alloy (b), and Al (c) (the curves in the graphs reflect the changes in localization-site positions with time).

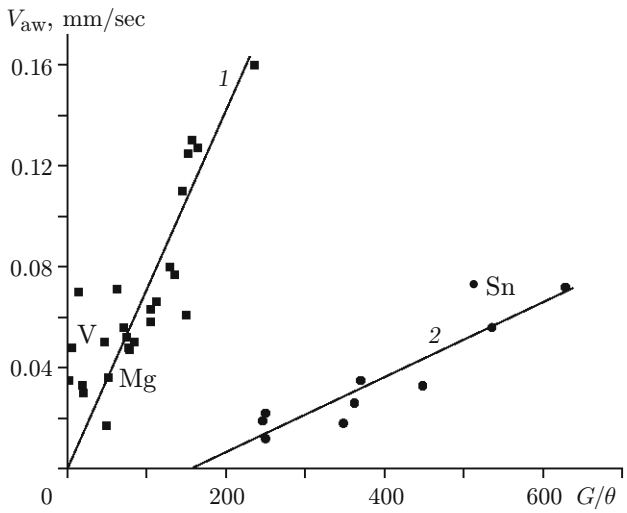


Fig. 4. Velocities of autowaves versus reduced hardening rates at the stage of linear hardening (1) and at the stages of light slipping (2).

$V_{II} = \Xi G/\theta$, where $G$ is the shear modulus of the material and $\Xi$ is a constant with the dimension of velocity, is shown in Fig. 4. The values of velocities of autowaves in the vanadium and magnesium alloys (curve 1) are in good agreement with this dependence. It was noted [15, 16] that the velocities of localization of autowaves in b.c.c. silicon iron and in the h.c.p. Zr–Nb alloy also obey this dependence. Hence, there are grounds to assume that this parameter is independent of the crystalline lattice type, structural state, chemical composition, and micromechanism of plastic shear; this parameter is determined by the balance of hardening and relaxation processes at the microscopic level, as was shown, e.g., in [14]. Additional evidence of the latter statement can be the data on the wave process of localization in tin. The deformation autowave velocity, as is seen from Fig. 4, is within the range of values extrapolated by curve 2 rather than curve 1. It was noted [14] that this group of points is composed by velocities of autowaves at the stages of easy slipping of single crystals and yield areas of polycrystalline samples. The main factor of resistance to deformation, which is the contact interaction of dislocations of various slipping systems, is absent in the stages considered; therefore, hardening is not large, and the lattice friction of dislocations plays the leading role [17]. At room temperature, tin deformation occurs under similar conditions. The re-crystallization threshold for tin is $T_R = 200$ K. Hence, for $T \approx 300$ K and small loading velocity of $8.3 \cdot 10^{-5}$ sec$^{-1}$, intense dynamic re-crystallization is developed; the dislocation barriers break down and do not exert any decelerating effect. The main contributions to resistance to deformation are made by lattice friction and by interaction of dislocations with grain boundaries. Yet, the contribution of deceleration of dislocations by grain boundaries is, apparently, small, as the grain size in Sn samples was greater than 1 mm (see Table 1).

In addition, the results of the present work allow us to conclude that, if the parabolic stage of the strain curve of the material consists of several substages, the spatially periodic steady structure is observed only if the hardening exponent is close to 1/2. After the end of stable deformation identified by Taylor [10], when $n$ becomes lower than 1/2, the zone of future fracture is identified, the amplitudes of deformation localization in the remaining sites decreases, and these sites move toward the point of fracture. Thus, it was possible to trace the transition of a spatially periodic steady localization pattern to a fracture neck. In these intervals, all previously formed deformation sites, except for one, move so (see, e.g., Fig. 3c) that their trajectories can be described by the system

$$(X_0)_i + V_i(t_f - t_0) = \text{const}, \tag{1}$$

where $(X_0)_i$ is the coordinate of an arbitrary site of deformation localization by the beginning of the stage with $n < 1/2$, $V_i$ is the velocity of this localization site, $t_f$ is the time from the beginning of deformation to fracture, and $t_0$ is the time from the beginning of deformation to the beginning of the stage with $n < 1/2$. The constant in these equations is the coordinate of the motionless localization zone $X_f$ where the fracture occurs in what follows. Formally, the velocity $V_i$ can be either positive or negative, depending on the direction of motion of the localization site. Hence, the following relation is valid for two arbitrary sites:

$$(X_0)_i - (X_0)_j = (V_j - V_i)(t_\mathrm{f} - t_0). \tag{2}$$

Obvious transformations (2) yield the dependence

$$t_\mathrm{f} = \Delta X_{ij}/(\Delta V_{ij} + t_0), \tag{3}$$

where $\Delta X_{ij}$ is the distance between two arbitrary localization sites at the beginning of the parabolic stage with $n < 1/2$ and $\Delta V_{ij}$ is the difference in their velocities. Based on these data, Eq. (3) allows one to determine the fracture time, i.e., the sample lifetime. On the other hand, knowing $t_\mathrm{f}$ and using Eq. (1), one can calculate the coordinate of the fracture point of the sample $X_\mathrm{f}$ even if the position of the motionless localization zone is unknown.

**Conclusions.** An analysis of the research performed allowed us to formulate the following general features of the development of localization in the plastic flow.

1. Autowaves of localized plasticity arise at the linear stages of the loading curves for metals and alloys, independent of the type of the crystalline lattice; the velocity of these waves is inversely proportional to the hardening coefficient normalized to the shear modulus.

2. At the parabolic stages corresponding to Taylor's stable strain hardening ($n \approx 1/2$), the patterns of macrolocalization of plastic deformation are presented by spatially periodic steady distributions of localization sites.

3. After Taylor's parabolic hardening, materials with b.c.c. and h.c.p. lattices display transitional stages with $n < 1/2$, which are finalized by the formation of a macroscopic neck with subsequent development of viscous fracture. The macrolocalization patterns corresponding to these stages are systems of moving deformation sites; the farther these sites from the point of future fracture, the higher the velocities of these sites. The point of future fracture is fairly early fixed by one localization zone incipient at the end of the stage of Taylor's hardening.

4. Formation of the neck of viscous fracture starts far before the fracture per se and results from correlated motion of the sites of localized plastic flow, leading to their "association" in the vicinity of the fracture point.

5. The kinetic characteristics of the sites of localized plasticity at the transitional stage allow one to predict the time and coordinates of the point of the sample fracture.

The authors are grateful to N. M. Rusin for the samples of submicrocrystalline aluminum.

This work was supported by the Russian Foundation for Basic Research (Grant No. 05-08-18248).

## REFERENCES

1. L. B. Zuev and V. I. Danilov, "A self-excited wave model of plastic deformation in solids," *Phil. Mag.*, **79**, No. 1, 43–57 (1999).
2. L. B. Zuev and V. I. Danilov, "Nature of large-scale correlations in a plastic flow," *Fiz. Tved. Tela*, **39**, No. 8, 1399–1403 (1997).
3. L. B. Zuev, "Wave phenomena in low-rate plastic flow of solids," *Ann. Phys.*, **11/12**, 965–984 (2001).
4. S. A. Barannikova, V. I. Danilov, and L. B. Zuev, "Localization of twinning plastic deformation in single crystals of annealed $\gamma$-Fe," *Zh. Tekh. Fiz.*, **72**, No. 9, 63–66 (2002).
5. L. B. Zuev, B. S. Semukhin, and N. V. Zarikovskaya, "Reconstruction of the autowave structure upon deformation of polycrystalline aluminum," *Tech. Phys.*, **46**, No. 5, 563–568 (2001).
6. E. Macherauch, "Plastische Deformation von Polykristallen," *Z. Metallkunde*, **55**, No. 2, 60–82 (1964).
7. V. S. Ivanova and V. A. Ermishkin, *Strength and Plasticity of Refractory Metals and Single Crystals* [in Russian], Metallurgiya, Moscow (1976).
8. V. I. Trefilov, I. D. Gornaya, V. F. Moiseev, et al., "Linear stage in strain hardening of polycrystalline body-centered cubic metals and alloys," *Dokl. Akad. Nauk Ukr. SSR, Ser. A*, No. 11, 81–85 (1982).
9. N. A. Koneva and É. V. Kozlov, "Physical nature of the stages of plastic deformation," in: *Structural Levels of Plastic Deformation and Fracture* [in Russian], Nauka, Novosibirsk (1990).
10. R. Honeycomb, *The Plastic Deformation of Metals*, Cambridge University Press, Cambridge (1968).
11. B. Jauol, "Etude de la forme des courbes de deformation plastigue," *J. Mech. Phys. Solids*, No. 2, 95–114 (1957).
12. V. I. Trefilov, V. F. Moiseev, and É. P. Pechkovskii, *Strain Hardening and Fracture of Polycrystalline Metals* [in Russian], Naukova Dumka, Kiev (1989).

13. T. M. Poletika, G. N. Narimanova, S. V. Kolosov, and L. B. Zuev, "Plastic flow localization in commercial zirconium alloys," *J. Appl. Mech. Tech. Phys.*, **44**, No. 2, 262–270 (2003).
14. L. B. Zuev, V. I. Danilov, and B. S. Semukhin, "Space–time ordering in plastic deformation of solids," *Usp. Fiz. Metal.*, **3**, No. 3, 237–304 (2002).
15. V. I. Danilov, G. V. Shlyakhova, L. B. Zuev, et al., "Stages of plastic flow and macrolocalization of deformation in Fe–3% Si polycrystals," *Fiz. Metal. Metalloved.*, **98**, No. 3, 107–112 (2004).
16. L. B. Zuev, V. I. Danilov, S. A. Barannikova, and I. Yu. Zykov, "Plastic flow localization as new kind of wave processes in solids," *Mat. Sci. Eng. A*, 319–321, 160–163 (2001).
17. V. I. Danilov, S. A. Barannikova, and L. B. Zuev, "Localized strain autowaves at the initial stages of plastic flow of single crystals," *Tech. Phys.*, **48**, No. 11, 1429–1435 (2003).